Earth, Planets and Space

FULL PAPER

Open Access

Seafloor hydrothermal alteration affecting magnetic properties of abyssal basaltic rocks: insights from back-arc lavas of the Okinawa Trough

Masakazu Fujii[1,2]*, Hiroshi Sato[3], Eri Togawa[3], Kazuhiko Shimada[4] and Jun-ichiro Ishibashi[4]

Abstract

Seafloor hydrothermal systems in the back-arc region of the Okinawa Trough have been viewed as a modern analogue to the Kuroko-type volcanogenic massive sulfide deposits. Detection of magnetic signatures is widely utilized and assumed to facilitate the understanding of geological controls on hydrothermal system genesis. However, the magnetic properties of seafloor volcanic rocks are still poorly understood because of the difficulties of sample acquisition. Here, we report rock magnetic data along with linked geochemical and petrological data of volcanic rock samples obtained from the Irabu knolls of the southern Okinawa Trough. Both fresh and hydrothermally altered basaltic andesites were successfully obtained from the seafloor via submersible. A fresh sample, with single-domain titanomagnetite grains, is strongly magnetized with NRM intensity of up to 100 A/m. Minute skeletal and dendritic titanomagnetite grains are also observed. A second fresh sample, with multi-domain titanomagnetite grains, contains a greater amount of titanomagnetite grains, but exhibits NRM intensity ~ 10 A/m at most. In contrast to the fresh samples, hydrothermally altered samples show extremely low NRM intensities along with low saturation magnetization and certain contribution of paramagnetic minerals. Grain assemblages of pyrite and chalcopyrite grains appear along cracks in the groundmass. Our results indicated that fine titanomagnetite grains in groundmass within back-arc lava flows are altered due to hydrothermal processes. The recorded primary remanent magnetization of the lava flows is thus partly removed by hydrothermal alteration. Magnetization reduction related to hydrothermal activity produces local crustal magnetization lows and thus enables us to detect hydrothermal alteration zones by utilizing magnetic field measurements in space. In particular, the lavas we examined (via their resultant basaltic andesites) have high Curie temperatures greater than 400 °C, which is significantly higher than those indicated by mid-ocean ridge basalts, suggesting that the thermal effect for crustal magnetization may be less in back-arc settings.

Keywords: Magnetic properties, Hydrothermal alteration, Titanomagnetite, Back-arc basaltic andesite, Okinawa Trough

*Correspondence: fujii.masakazu@nipr.ac.jp
[1] National Institute of Polar Research, 10-3 Midoricho, Tachikawa, Tokyo 190-8518, Japan
Full list of author information is available at the end of the article

Fujii *et al. Earth, Planets and Space*   (2018) 70:196

Page 2 of 14

Introduction

Hydrothermal activity in the back-arc region of the Okinawa Trough has been recognized as a modern analogue to the Kuroko-type volcanogenic massive sulfide deposits since its first discovery in 1989 (Halbach et al. 1989). The Okinawa Trough is located behind the Ryukyu arc–trench system and is characterized by active rifting structures and magmatism along the depression. It is believed to represent a transitional stage between rifting and initial spreading (e.g., Sibuet et al. 1987). Tectonic settings, such as the Okinawa Trough, are assumed to sustain favorable conditions for the development of seafloor hydrothermal systems. More than ten hydrothermal vent fields have been discovered along a north–south transect of the Okinawa Trough (e.g., Ishibashi et al. 2015); however, there has been limited discussion on the geological controls for the genesis of hydrothermal systems.

Magnetic anomalies occurring near the seafloor can provide vital information for understanding the development of hydrothermal systems, such as the location, spatial extent, and mineralization histories of these systems. Because magnetic minerals are created, oxidized, and transformed, during hydrothermal processes, the mineralogical composition of hydrothermal systems provide direct evidence of the evolution of these systems. Reduced magnetization related to hydrothermal processes has been widely observed in volcanic rock-hosted hydrothermal fields located within arc and back-arc settings as well as at mid-ocean ridges (e.g., Tivey et al. 1993; Caratori-Tontini et al. 2012; Honsho et al. 2013; Fujii et al. 2015; Fujii and Okino 2018). Titanomagnetites are altered into less magnetic minerals such as titanomaghemite, titanohematite, and pyrite by contact with circulating, acidic hydrothermal fluid beneath the vent sites. Early studies into the magnetic properties of basalt from terrestrial lava outcrops (Ade-Hall et al. 1971), the ocean floor (Irving 1970; Watkins and Johnson 1971), ocean crustal drilling sites (Ade-Hall et al. 1973), and laboratory experiments (Johnson and Merrill 1972, 1973) have demonstrated that magnetization is significantly affected by low-temperature oxidation (maghemitization), in which the initial titanomagnetite is altered to titanomaghemite. With more extreme alteration, titanomagnetite pseudomorphs change into titanohematite grains (Ade-Hall et al. 1971). Clues for understanding the behavior of magnetic minerals relative to hydrothermal activity within oceanic crust were obtained from a massive sulfide body in the Troodos Ophiolite complex in Cyprus. This investigation was based on the results of a magnetic survey that revealed a strong, low magnetic field over a stockwork zone hosted within in a basaltic sequence (Johnson et al. 19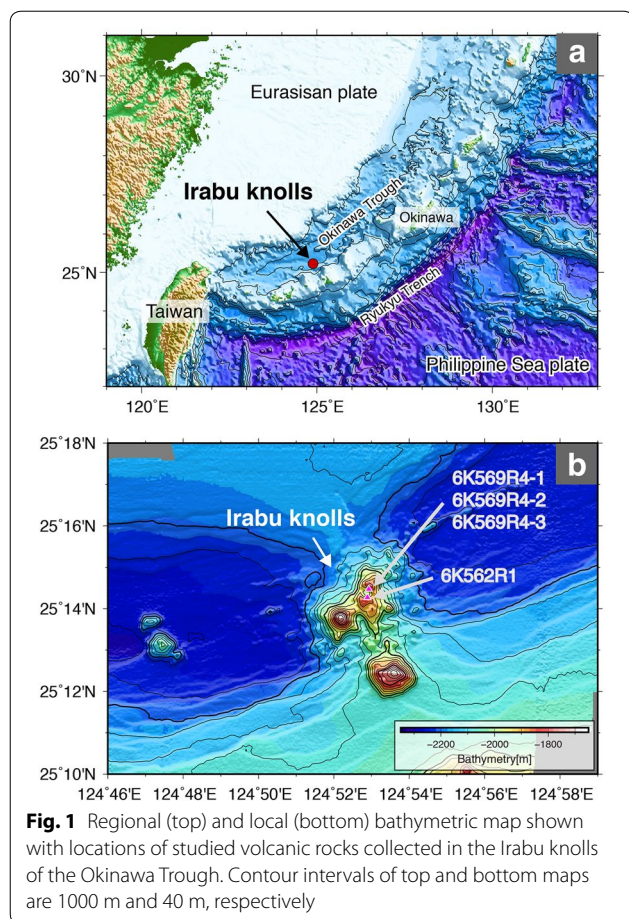82). Studies by Hall (1992) have also revealed that titanomagnetite in the basaltic basement of this area has been replaced by non-magnetic sulfide minerals, and that the basalt itself has been altered to a clay, silica, and chlorite assemblage within the stockwork up-flow zone. Though reduced magnetization related to hydrothermal processes within basaltic rock is well established and utilized for characterizing hydrothermal systems, studies that use the alteration of magnetic rocks to understand such magnetic lows are limited for mid-ocean ridges. Moreover, the effect of seafloor hydrothermal alteration on abyssal basaltic rocks is still poorly understood because it remains difficult to acquire geological samples from the deep sea. To expand magnetic surveys near the seafloor in the Okinawa Trough and to establish benchmarks for interpreting magnetic data from seafloor basalts, material study of such basalts is essential.

Here, we report rock magnetic, geochemical, and petrological results of volcanic rocks obtained from the Irabu knolls of the southern Okinawa Trough. Both fresh and altered samples were successfully obtained from the seafloor via submersible. Our newly generated and comprehensive dataset clearly reveals a relationship between the magnetic characteristics of lava flows and sulfide mineralization due to hydrothermal alteration.

Materials and methods

Basaltic rocks obtained from the Irabu knolls in the southern Okinawa Trough were utilized in this study. The Okinawa Trough is a back-arc basin setting located along the eastern margin of the Eurasian continent, which is characterized by active rifting structures and magmatism along the depression (e.g., Letouzey and Kimura 1986; Fig. 1a). The Irabu knolls occur at the axial segment boundary of the back-arc rift zone in the southern Okinawa Trough (25°14′N, 124°53′E; Fig. 1b). Rock samples were collected from a northeast knoll with depression structure of the Irabu knolls during the R/V *Yokosuka* YK00-06 leg2 cruise in 2000 (Figs. 1b, 2). Studied four samples were obtained by using the submersible *Shinkai 6500* during dive surveys of #562 and #569. The 6K#562R1 sample was collected at the bottom of northern slope (Table 1; Figs. 1b, 2a, b). Both altered and fresh rock samples were collected from the same location of the bottom of southern slope and were named as 6K#569R4-1, 6K#569R4-2, and 6K#569R4-3 (Table 1; Figs. 1b, 2c–h).

To characterize the petrological signatures and rock magnetic properties of the samples, a detailed dataset of mineral texture and composition, whole-rock chemical composition, magnetic properties, and bulk grain density (ρ) was constructed. Magnetic properties included: natural remanent magnetization (NRM) intensity, magnetic susceptibility, hysteresis parameters, Curie temperature,

Fujii *et al. Earth, Planets and Space*   (2018) 70:196

Page 3 of 14

Fig. 1 Regional (top) and local (bottom) bathymetric map shown with locations of studied volcanic rocks collected in the Irabu knolls of the Okinawa Trough. Contour intervals of top and bottom maps are 1000 m and 40 m, respectively

and Ti content (x) of titanomagnetite grain ($Fe_{3-x}Ti_xO_4$). Cubic subsamples (8 cm³), several small chip subsamples, and large massive subsamples were systematically cut from whole-rock samples including surface to interior parts. The cubic subsamples were used for NRM, magnetic susceptibility, and bulk grain density measurements. Small chip subsamples (30–70 mg) were used for thermomagnetic experiments in high-temperature conditions. Large chip subsamples (180–480 mg) were used for magnetic hysteresis analyses, primarily for saturation magnetization measurements. Large chip subsamples were also used for thin sections and whole-rock geochemical analysis. Sample 6K#569R4-3 is light gray-colored angular sparsely phyric volcanic rock. Although the surface and peripheral zone of the sample has yellowish altered portion, glassy chilled margin remains as relatively unaltered area. To examine the effect of the heterogeneous alteration on magnetism, we took two cubes and two chips from the altered surface, and three cubes and five chips from the unaltered chilled margin.

Polished thin sections were analyzed by polarization microscope and electron microprobe (JEOL JXA-8530F) at Kyushu University. Mineral type, texture, and distribution for silicate minerals were observed by transmitted light microscopy, and metal oxides and sulfides were observed by reflected light microscopy. Wavelength-dispersive X-ray spectroscopy (WDS) was used for composition measurements and set to an acceleration voltage of 20 kV and a probe current of 10 nA. Compositions of sulfide minerals were analyzed for altered samples along with sulfide grains, and those of silicate and metal oxides were analyzed for fresh samples.

The major element compositions of bulk rock samples were determined using X-ray fluorescence (XRF, Rigaku Supermini) spectrometer at Senshu University. Prior to analysis, samples were dried at 950 °C followed by melting at 1200 °C in a mixture consisting of 0.9000 g powdered sample and 4.5000 g lithium tetraborate ($Li_2B_4O_7$) flux. Calibrations were conducted using the methods reported by Sato (2010).

The NRM intensity was measured for all cubic subsamples via spinner magnetometer installed in (D-SPIN, Natsuhara Giken) at the Center for Advanced Marine Core Research (CMCR) of Kochi University. Stepwise alternating field demagnetizations (AFDs) of NRM for the representative cube specimen of each sample were performed in 0–180 mT using an automatically rotated demagnetizer (D-SPIN, Natsuhara Giken) installed in CMCR. The magnetic susceptibility was measured for all cubic subsamples using the AGICO KLY-3 Kappabridge at CMCR. High-temperature experiments were performed on chip subsamples from all original rock samples. Saturation magnetization was measured under an inducing magnetic field of 0.5 T in a vacuum condition (1 Pa) by using a magnetic balance (Natsuhara Giken MNB-89) at CMCR. The specimens were heated from room temperature to 700 °C and cooled back to 50 °C at a rate of 10–12 °C/min. The Ti substitution (x) for titanomagnetite grains ($Fe_{3-x}Ti_xO_4$) in fresh samples with a major Curie temperature is estimated using measured Curie temperature (T_C) based on the following best-fit equation: $T_C = 575 - 552.7 x - 213.3 x^2$ (Hunt et al. 1995), in which the end members are magnetite ($x = 0$) and ulvöspinel ($x = 1$). Magnetic hysteresis parameters were measured on several chip subsamples ($N = 3$–7) for each original sample by using a vibrating sample magnetometer (VSM) at CMCR. The ratio of saturation remanent magnetization (Mrs) to saturation magnetization (Ms) against the ratio of coercivity of remanence (Hcr) to bulk coercivity (Hc) was used to evaluate the ferromagnetic grain size in rock samples based on the Day plot (e.g., Day et al. 1977). Bulk grain density was measured on all cubic subsamples using a high-precision microbalance with a resolution of 0.01 mg and a gas pycnometer (AccuPycTM 1330 Pycnometer) at

Fujii *et al. Earth, Planets and Space* (2018) 70:196

Page 4 of 14
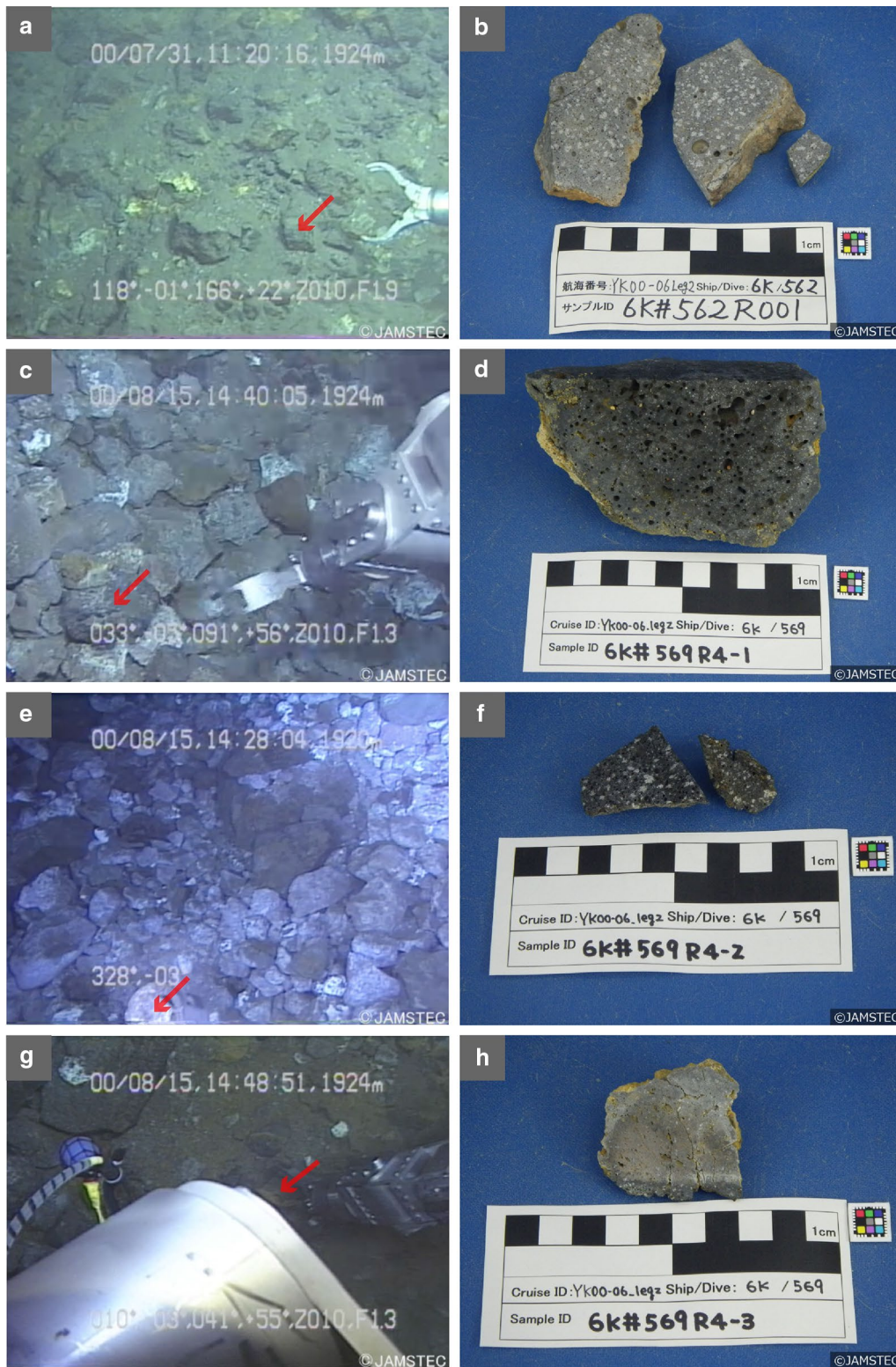
Fig. 2 Photographs of outcrop (left) and samples (right) of studied volcanic rocks collected in the Irabu knolls of the Okinawa Trough; 6K#562R1 (**a** and **b**), 6K#569R4-1 (**c** and **d**), 6K#569R4-2 (**e** and **f**), and 6K#569R4-3 (**g** and **h**)

Fujii *et al. Earth, Planets and Space* (2018) 70:196

Page 5 of 14

Table 1 Location and sampling details of the studied volcanic rock samples from the Irabu knolls of the Okinawa Trough; 6K#562R1, 6K#569R4-1, 6K#569R4-2, and 6K#569R4-3

| Sample name	Latitude (°N)	Longitude (°E)	Depth (m)	Sampling date	Sampling size (cm)	Weight (kg)
6K#562R1	25.2379	124.8815	1924	31 Jul 2000	16.0 × 14.0 × 9.5	2.0
6K#569R4-1	25.2412	124.8821	1921	15 Aug 2000	13.5 × 12.5 × 11.5	1.65
6K#569R4-2	25.2412	124.8821	1921	15 Aug 2000	14 × 8 × 7	0.85
6K#569R4-3	25.2412	124.8821	1921	15 Aug 2000	14 × 7.5 × 6.5	0.5

the Atmosphere and Ocean Research Institute (AORI), University of Tokyo.

Petrography and whole-rock geochemistry

Based on microscopic observation and whole-rock geochemical analysis, studied volcanic rocks were identified as fresh (6K#562R1 and 6K#569R4-2), partly altered (6K#569R4-3), and altered basaltic andesite (6K#569R4-1). Freshness, or degree of alteration, was determined based on alteration of primary silicate minerals and existence of secondary calcite under microscopic observation and chemical index loss on ignition (LOI). The LOI, which measures the change in mass after heating at 950 °C, is one of the indicators of alteration, and it is roughly correlated with contents of secondary precipitation minerals during alteration (Haraguchi et al. 2014). The content of LOI was high in samples 6K#569R4-1 and 6K#569R4-3.

Sample 6K#562R1 is light gray-colored angular plagioclase–phyric basaltic andesite. Surface and vesicles up to 1 cm in diameter of collected samples are rimmed by yellowish altered portion. Groundmass exhibited an intergranular texture, and phenocrysts were mainly glomeroporphyritic plagioclase with minor amounts of clinopyroxene (Fig. 3A). Under microscopic observation, it contains both skeletal and elongated titanomagnetite, which is seen as metallic, white grains in thin section under reflected light (Fig. 3B). Titanomagnetite grains,
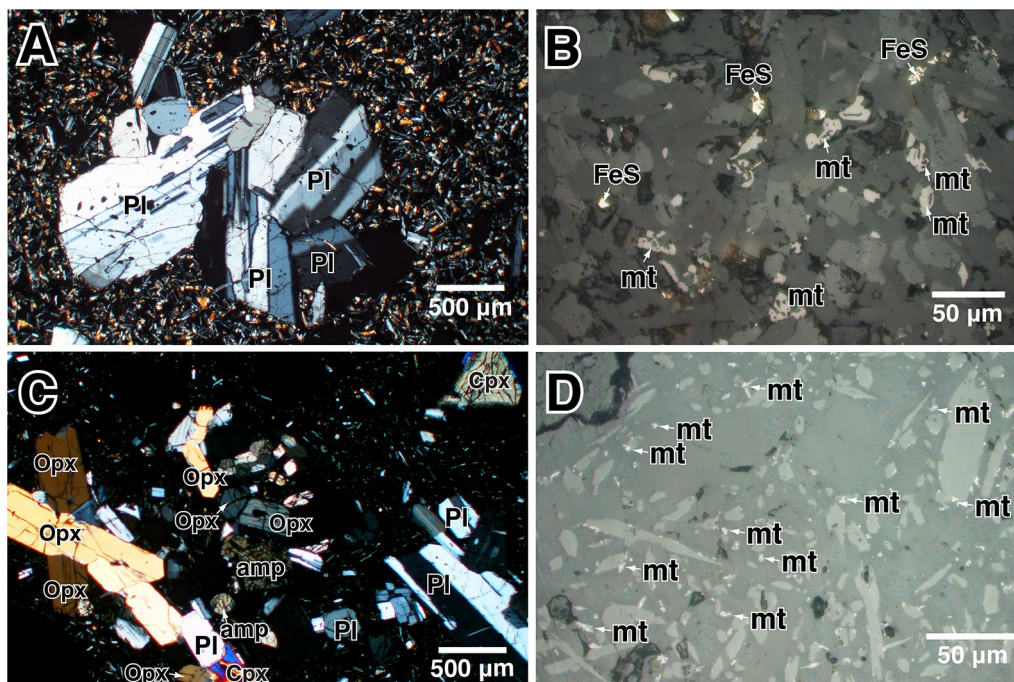
Fig. 3 Photomicrographs of the studied fresh volcanic rock samples from the Irabu knolls of the Okinawa Trough; 6K#562R1 and 6K#569R4-2. **A** Plagioclase (Pl) glomeroporphyritic and intergranular groundmass texture in the 6K#562R1. Under transmitted crossed polarized light (CPL). **B** Titanomagnetite (mt) and pyrite (FeS) grains in the 6K#562R1. Under reflected plane-polarized light (PPL). **C** Plagioclase (Pl), orthopyroxene (Opx), amphibole (amp), and clinopyroxene (Cpx) glomeroporphyritic and intersertal groundmass texture in the 6K#569R4-2. Under transmitted CPL. **D** Titanomagnetite (mt) grains in the 6K#569R4-2. Under reflected PPL

Fujii *et al. Earth, Planets and Space* (2018) 70:196

Page 6 of 14

with widths of less than a few microns to tens of microns, were scattered within the groundmass of this sample. Results of electron microprobe analysis (EPMA) revealed an average composition for the titanomagnetite magnetite grains of $Fe^{2+}_{1.28}Mg_{0.04}Fe^{3+}_{1.18}Ti_{0.33}Al_{0.12}O_4$ within thin section ($N = 11$). Yellowish iron sulfides were also observed in thin section of this sample (Fig. 3B). EPMA revealed a pyrite composition for the iron sulfides (FeS_2); the atomic weight ratio of S/Fe was 1.94–2.03 ($n = 7$).

Sample 6K#569R4-1 is dark-colored highly porous subangular basaltic andesite. Calcite was secondary developed within vesicles. Under microscopic observation, brownish alteration halos were developed in groundmass (Fig. 4A). Groundmass exhibited an intersertal texture, and phenocrysts were mainly glomeroporphyritic plagioclase with minor amounts of clinopyroxene (Fig. 4B). It does not contain titanomagnetite, but both pyrite and a lesser amount of chalcopyrite are present. Angular pyrite grains were scattered within the groundmass mainly within alteration halos (Fig. 4C). Assemblages of pyrite grains ranged from 50 to 100 μm in width. EPMA revealed a pyrite composition of FeS_2; the atomic weight ratio of S/Fe was 1.97–2.04 ($n = 10$). Yellowish to white grains were also observed, but their composition was similar to yellowish pyrite grains. One chalcopyrite grain (Fig. 4D) was enough size for analysis and it has $Fe_{0.96}Cu_{0.94}S_2$. Calcite was secondary developed within amygdale.

Sample 6K#569R4-2 is dark-colored highly porous subangular plagioclase–phyric basaltic andesite. Groundmass exhibited an intersertal texture, and phenocrysts were mainly glomeroporphyritic plagioclase with minor amounts of orthopyroxene, amphibole, and clinopyroxene (Fig. 3C). No secondary minerals fill vesicles, and alteration portions are not observed on the surface of sample under macroscopic view. It contains both skeletal and dendritic titanomagnetite (Fig. 3D). Minute titanomagnetite grains were scattered in the groundmass with widths ≤ 10 μm. Because it was difficult to obtain enough spot area for analysis even under the minimum beam diameter of the EPMA system, only three titanomagnetite grains were analyzed by EPMA with an average composition of $Fe^{2+}_{1.17}Mg_{0.11}Fe^{3+}_{1.25}Ti_{0.29}Al_{0.14}O_4$. No iron sulfides were confirmed in thin section of this sample.

Sample 6K#569R4-3 is light gray-colored angular sparsely phyric basaltic andesite. Although surface and peripheral zone of the sample have yellowish altered portion, glassy chilled margin remains as relatively unaltered area. Under microscopic observation, groundmass is mostly brown-colored particularly along alteration halos (Fig. 4E). Subsamples for thin-section observation and EMPA and XRF analyses were

collected from altered area. Groundmass exhibited an intersertal texture, and phenocrysts were mainly glomeroporphyritic plagioclase with minor amounts of orthopyroxene and clinopyroxene (Fig. 4F). It contains the yellowish iron sulfides pyrite in altered areas. Pyrite grains were scattered in the groundmass mainly along fractures with alteration halos (Fig. 4G) and fracture of primary silicate mineral (Fig. 4H). Grain assemblages of pyrite range up to approximately 500 μm in width. EPMA for altered area revealed a pyrite composition of FeS_2; the atomic weight ratio of S/Fe was 1.89–2.03 ($n = 26$). Yellow to white grains were also observed, but composition is similar to yellowish pyrite grains. Titanomagnetite grains were observed only in a relatively unaltered area. Titanomagnetite grains form both skeletal and dendritic features (Fig. 4I, J).

Whole-rock geochemistry reveals that collected rock samples were basaltic andesites (Table 2). The Fe_2O_3 and TiO_2 content of all measured samples showed similar values ranging 9.9–10.7 wt% and 0.65–0.79 wt%, respectively. The CaO content of partly altered and altered samples exhibited relatively low values of < 8 wt%, and the K_2O content of 6K#569R4-1 was lower than that of the other samples. These compositions are consistent with chemical changes that occur during hydrothermal alteration in which Ca and K are leached from basaltic rocks (e.g., Mottle and Holland 1978).

Magnetic properties

The NRM intensity and magnetic susceptibility of studied samples were measured on cubic subsamples ($N = 3$–5) and exhibited $0.8 - 88.7$ A/m and $0.0021 - 0.0607$ (SI), respectively (Table 3; Fig. 5a; Additional file 1: Table S1). Low-field magnetic susceptibility is primarily a proxy or the concentration (and grain size) of ferromagnetic minerals, with lesser contributions from paramagnetic minerals. The sample of 6K#569R4-1 has remarkably low values of NRM and magnetic susceptibility. The Koenigsberger ratio (Q), which is the proportion of NRM to induced magnetization, of all samples ranged from 7 to 202 with an assumed external magnetic field of 40,000 nT, indicating that the magnetization is dominated by remanence ($Q > 1$). Stepwise AFD of NRM for representative cube specimens of all samples showed that a stable primary remanence component was recognized in 6K#569R4-2 and 6K#569R4-3 (Fig. 6a, b). This remanent magnetization is likely a primary thermal remanent magnetization (TRM) carried by titanomagnetite grains. The AFD result for NRM of 6K#562R1 shows two components: One diminishes at less than 20 mT and the other remains in up to 180 mT (Fig. 6c). This probably results in bimodal size and shape distribution of coarse grains
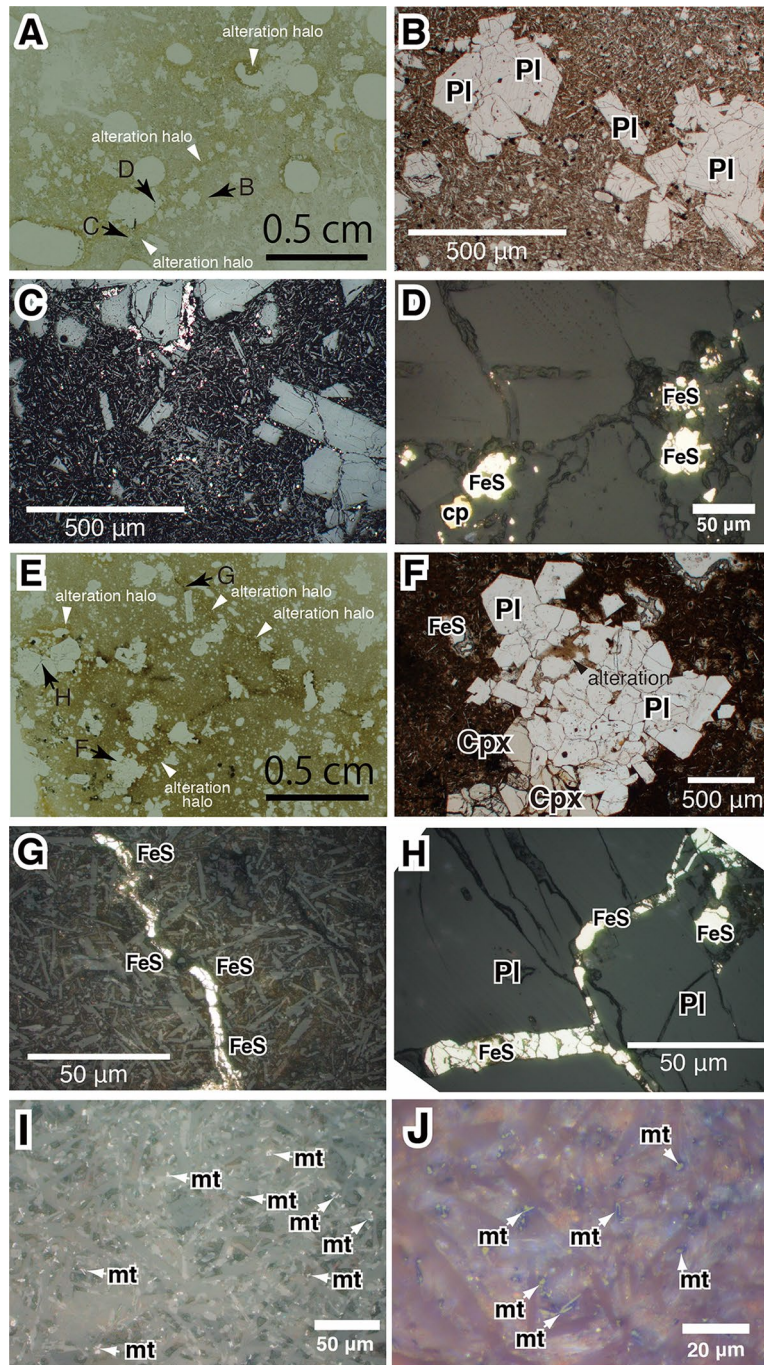
Fig. 4 Photomicrographs of the studied altered volcanic rock samples from the Irabu knolls of the Okinawa Trough: 6K#569R4-1 and 6K#569R4-3; **A** thin-section image of 6K#569R4-1 under transmitted reflected plane-polarized light (PPL). Arrows in **B**, **C**, and **D** are approximate positions of the following photographs. **B** Plagioclase (Pl) glomeroporphyritic and intersertal groundmass texture in the 6K#569R4-1. Small black minerals scattered within groundmass are pyrite. Under transmitted PPL. **C** Mode of occurrence of pyrite grains in the 6K#569R4-1. All bright grains are pyrite grains. Under reflected PPL. **D** Pyrite (FeS) and chalcopyrite (cp) grains in the 6K#569R4-1. Under reflected PPL. **E** Thin-section image of 6K#569R4-3 under transmitted PPL. Arrows in **F**, **G**, and **H** are approximate positions of the following photographs. **F** Plagioclase (Pl) and clinopyroxene (Cpx) glomeroporphyritic and intersertal groundmass texture in the 6K#569R4-3. Plagioclase is partly altered. Under transmitted PPL. **G** Bright light yellowish pyrite grains form veinlet along fracture in groundmass of the 6K#569R4-3. Under reflected PPL. **H** Bright light yellowish pyrite grains form veinlet along fracture in plagioclase (Pl) phenocryst of the 6K#569R4-3. Under reflected PPL. **I** and **J** Titanomagnetite (mt) grains in the 6K#569R4-3. Under reflected PPL (**J**: oil immersion)

Table 2 Whole-rock geochemistry of the studied volcanic rock samples from the Irabu knolls of the Okinawa Trough; 6K#562R1, 6K#569R4-1, 6K#569R4-2, and 6K#569R4-3

Sample name	SiO$_2$	TiO$_2$	Al$_2$O$_3$	Fe$_2$O$_3$*	MnO	MgO	CaO	Na$_2$O	K$_2$O	P$_2$O5	Total	H$_2$O– (%)	LOI** (%)
6K#562R1	52.1	0.65	18.3	10.0	0.16	4.2	11.2	2.15	0.33	0.09	99.2	0.51	0.35
6K#569R4-1	53.9	0.78	17.7	10.7	0.28	5.0	7.1	2.18	0.12	0.11	97.9	4.24	3.65
6K#569R4-2	54.9	0.74	17.9	9.9	0.17	3.4	9.4	2.61	0.64	0.11	99.7	0.57	− 0.07
6K#569R4-3	54.8	0.79	17.9	10.1	0.18	3.4	7.9	2.86	0.54	0.11	98.6	1.96	2.69

*Total Fe measured as Fe2O3

**Loss on ignition

in phenocryst and fine skeletal and elongated grains in the groundmass. No fine lamellae within coarse titanomagnetite grains were identified during our observation of our polarization and electron microscopes at least. The NRM of 6K#569R4-1 shows instability with gradual curvature and mostly demagnetized at 70 mT (Fig. 6d). Instability of NRM was observed in all samples especially at less than 5 mT, which is probably due to secondary remanence during or after sampling.

The NRM and susceptibility (K) of 6K#562R1 and 6K#569R4-2 samples do not vary significantly within each sample as shown by their relative standard deviations (SD_{NRM} = 7–25% and SD_K = 3–9%; Table 3). In contrast, 6K#569R4-1 and 6K#569R4-3 exhibit substantial heterogeneity within specimens (Table 3), with large relative standard deviations of NRM (SD_{NRM} = 57–59%) and susceptibility (SD_K = 37–40%). Grain density values ranged from 2.71 to 2.89 g/cm^3, with a maximum standard error of 0.04 (Table 3; Additional file 1: Table S1).

Thermomagnetic analyses for 6K#562R1 and 569R4-2 revealed a single Curie temperature of ∼ 420 °C (Table 3; Fig. 5c, e; Additional file 2: Table S2). Their warming and cooling curves were almost identical, thus indicating that low-temperature oxidation (maghemitization) did not occur in these samples. This results support mineralogical observation showing fresh signature and existence of titanomagnetite grains. The estimated ulvöspinel content (x in Fe$_{3-x}$Ti$_x$O$_4$) for 6K#562R1 and 569R4-2 shows 0.26. The thermomagnetic curve of 6K#569R4-3 exhibits a higher single Curie temperature of ∼ 540 °C, but warming and cooling curves differ (Table 3; Fig. 5d). The sample 6K#569R4-3 has two types of thermomagnetic curves. The first shows a single Curie temperature of ∼ 540 °C (equivalent to x of 0.06 in Fe$_{3-x}$Ti$_x$O$_4$), but warming and cooling curves slightly differ (Table 3; Fig. 5d). This signature is observed in unaltered part of the sample. The second curve is characterized by a hump in heating curves from 400 °C to 500 °C (Fig. 5d), while heating and cooling curves are markedly different; these characteristics are indicative of titanomaghemite grains, which are formed from titanomagnetite after low-temperature oxidation.

This signature is observed in altered part of the sample. The chip subsample that exhibited this oxidized signature shows extremely low saturation magnetization of 0.05 Am^2/kg. Sample 6K#569R4-1 exhibits a low signal for saturation magnetization and has Curie temperatures of ∼ 580 °C and ∼ 680 °C in heating, with a cooling curve that exhibits one additional Curie temperature of ∼ 300 °C (Fig. 5e).

The remanence ratio (Ms/Mrs) and coercivity ratio (Hcr/Hc) varied among samples of 6K#562R1, 6K#569R4-1, 6K#569R4-2, and 6K#569R4-3: 0.1–0.5 of Ms/Mrs and 1.1 to 3.5 of Hcr/Hc. Values of magnetic hysteresis parameters plot in broad area of the single-domain (SD) to pseudo-single-domain (PSD) region in the Day plot (Fig. 5b; Additional file 3: Table S3; Additional file 4: Figure S1). The saturation magnetization normalized to mass (Ms), which is a proxy for the concentration of ferromagnetic minerals, was 0.03–1.81 Am^2/kg among all samples (Fig. 5b). The Ms values are consistent with magnetic susceptibility; i.e., samples with larger Ms carry larger susceptibility. Data except for altered samples (6K#569R4-1 and part of 6K#569R4-3) are distributed along the mixing curves of single-domain (SD) and multi-domain (MD) magnetites (Dunlop 2002). The 6K#569R4-3 shows two characteristics: Specimens from unaltered part show high Ms (0.74–1.86 Am^2/kg, n = 5) and specimens from altered part show low Ms (0.05 Am^2/kg, n = 2). Typical examples of hysteresis curves are presented in Fig. 5c–f. Sample 6K#569R4-2 exhibits a contribution of SD grains (Fig. 5b, c). In contrast, 6K#562R1 displays a larger contribution of MD grains (Fig. 5b, e). Intermediate hysteresis signature between SD and MD grains is shown in 6K#569R4-3 (Fig. 5b, d). Specimens from the rock margins of sample 6K#569R4-3 show certain contribution of paramagnetic minerals (Fig. 5d). Sample 6K#569R4-1 also appears to be paramagnetic (Fig. 5f).

Discussion

The investigated back-arc basaltic andesites from the Irabu knolls display both fresh and altered signatures. Mode of occurrence of pyrite grains in partly
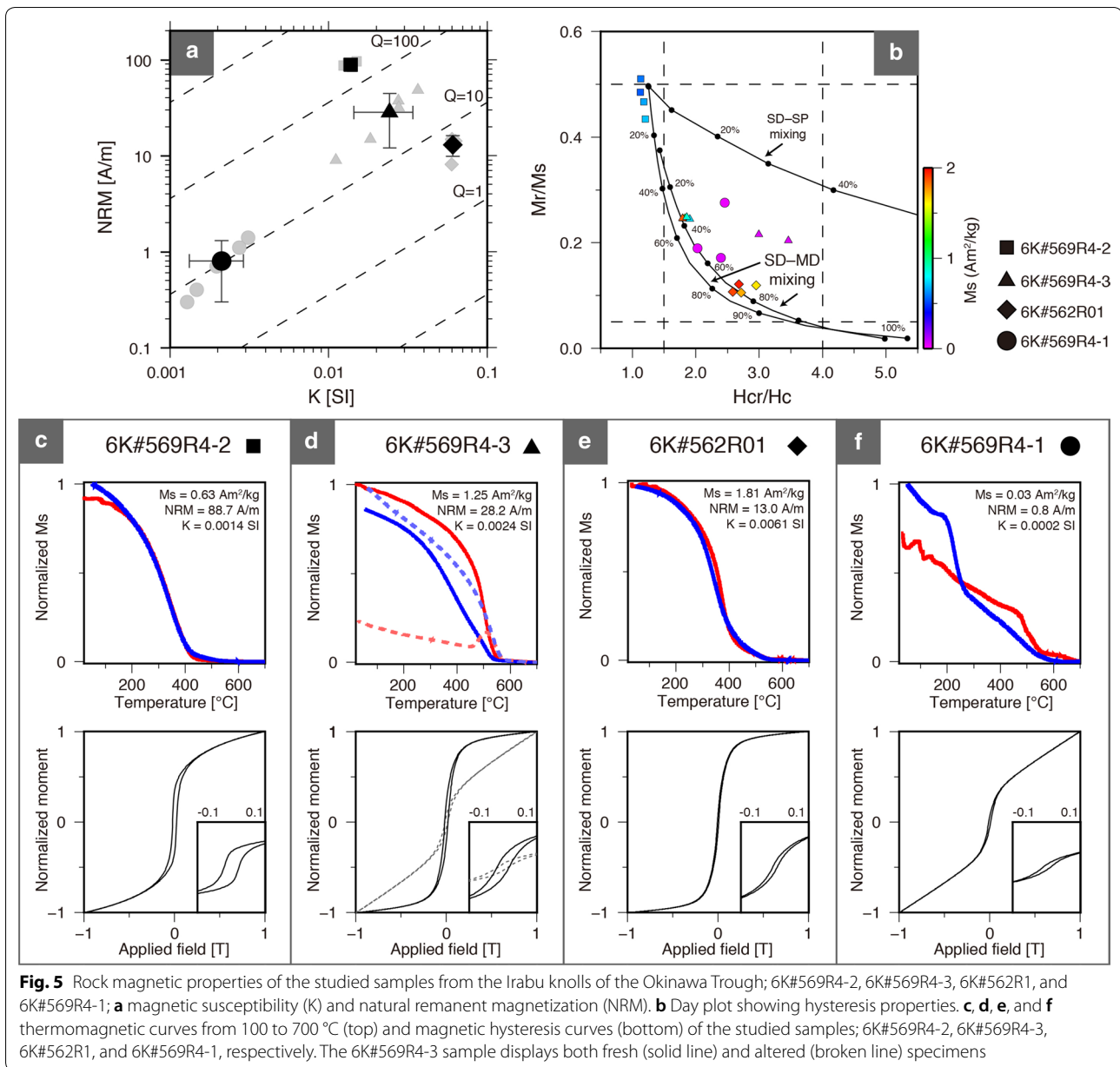
Fujii *et al. Earth, Planets and Space* (2018) 70:196

Page 9 of 14

Table 3 Rock magnetic properties and bulk grain density of the studied volcanic rock samples from the Irabu knolls of the Okinawa Trough; 6K#562R1, 6K#569R4-1, 6K#569R4-2, and 6K#569R4-3

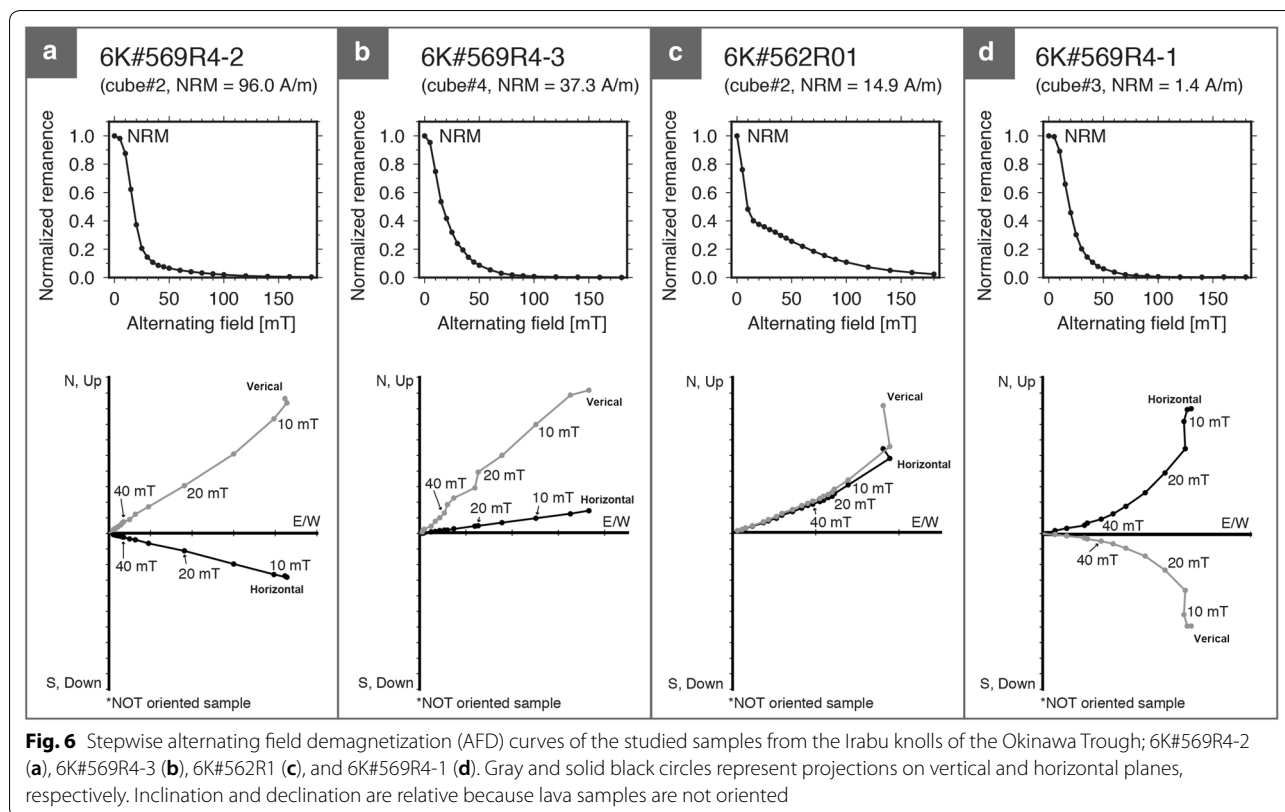| Sample name	ρ (kg/m^3)	$\sigma\rho$ (kg/m^3)	NRM (A/m)	σNRM (A/m)	K (SI)	σK (SI)	Q	T_c (°C)	x	Ms (Am^2/kg)	Rep. Hcr/Hc	Rep. Mrs/Ms	Magnetic domain state
6K#562R1	2.89	0.01	13.0	3.2	0.0607	0.0016	7	420	0.26	1.81	2.72	0.10	PSD
6K#569R4-1	2.71	0.04	0.8	0.5	0.0021	0.0008	12			0.03	2.40	0.17	PSD
6K#569R4-2	2.85	0.02	88.7	6.5	0.0138	0.0013	202	420	0.26	0.63	1.18	0.47	SD
6K#569R4-3	2.89	0.01	28.2	16.2	0.0242	0.0098	37	540	0.06	1.25	1.83	0.24	PSD

ρ, bulk grain density. $\sigma\rho$, standard deviation of ρ. NRM, natural remanent magnetization. σNRM, standard deviation of NRM. K, magnetic susceptibility. σK, standard deviation of K. Q, Koenigsberger ratio. T_c, Curie temperature. x, titanium content of Fe$_{3x}$Ti$_x$O$_4$ estimated from Curie temperature

Ms saturation magnetization, Hcr remanent coercivity, Hc coercivity, Mr saturation remanent magnetization, Rep representative

Fujii *et al. Earth, Planets and Space* (2018) 70:196

Page 10 of 14

Fig. 5 Rock magnetic properties of the studied samples from the Irabu knolls of the Okinawa Trough; 6K#569R4-2, 6K#569R4-3, 6K#562R1, and 6K#569R4-1; **a** magnetic susceptibility (K) and natural remanent magnetization (NRM). **b** Day plot showing hysteresis properties. **c**, **d**, **e**, and **f** thermomagnetic curves from 100 to 700 °C (top) and magnetic hysteresis curves (bottom) of the studied samples; 6K#569R4-2, 6K#569R4-3, 6K#562R1, and 6K#569R4-1, respectively. The 6K#569R4-3 sample displays both fresh (solid line) and altered (broken line) specimens

altered (6K#569R4-3) and altered (6K#569R4-1) basaltic andesite, in which they were scattered within the groundmass mainly along alteration halos, suggests that these pyrite grains were crystallized from solution during alteration. Samples affected by alteration lack fine titanomagnetite grains in groundmass. The existence of chalcopyrite grains in 6K#569R4-1 (Fig. 4D) signifies the influence of high-temperature hydrothermal fluid with > 250–300 °C (e.g., Hannington et al. 1995). Also, it is highly possible that this alteration is hydrothermal alteration judging from proximity of sampling sites to hydrothermal vents (Fukuba et al. 2015). High-temperature

hydrothermal alteration occurs when existing components become unstable under changing physical and chemical conditions (generally into > 250 °C, which is close to critical temperature of seawater in deep), and promotes alteration of primary minerals to more stable minerals and formation of secondary minerals under low water–rock ratio (rock-dominant) condition (e.g., Alt 1995). Results of comprehensive magnetic and petrological analyses demonstrate a clear relationship between magnetic properties and petrography related to alteration processes. Bulk rock geochemistry reveals that all samples are classified as basaltic andesite with similar

Fujii *et al. Earth, Planets and Space* (2018) 70:196

Page 11 of 14

Fig. 6 Stepwise alternating field demagnetization (AFD) curves of the studied samples from the Irabu knolls of the Okinawa Trough; 6K#569R4-2 (**a**), 6K#569R4-3 (**b**), 6K#562R1 (**c**), and 6K#569R4-1 (**d**). Gray and solid black circles represent projections on vertical and horizontal planes, respectively. Inclination and declination are relative because lava samples are not oriented

iron and titanium content. Due to this observed uniformity of geochemistry (Table 2), erupted magma difference as shown in Gee and Kent (1997) can be ignored for discussing the effects of hydrothermal alteration for these samples.

Based on petrological and magnetic analysis, SD-like and MD-like end members for fresh volcanic samples were identified. The sample 6K#569R4-2 is strongly magnetized, and exhibits NRM intensity 88.7 A/m in average (Fig. 5a). Ferromagnetic minerals in this sample display fresh (non-oxidized and/or non-altered) titanomagnetite with a SD-like magnetic domain state (Fig. 5b). Minute skeletal and dendritic titanomagnetite grains can be observed in the corresponding thin section (Fig. 3D). The Curie temperature is 420 °C (Fig. 5c), which is generally higher than those observed in mid-ocean ridge basalts (Gee and Kent 1997; Zhou et al. 2001). A low ulvöspinel content (x in $Fe_{3-x}Ti_xO_4$) of 0.26 is also displayed from the Curie temperature values. This is consistent with the average composition of titanomagnetite grains revealed by EPMA measurements. The estimated amount of titanomagnetite grains (m), which is based on the empirical equations with a linear relationship between Ms and x as follows: $m = Ms/(Ms \times 92 \times (1 - 1.23\ x))$ (Hunt et al. 1995), shows 1.0 wt%. Another fresh sample, 6K#562R1, shows a more MD-like magnetic domain state (Fig. 5b).

Size of titanomagnetite grains observed in thin section is much larger than those in sample 6K#569R4-2 (Fig. 3B). Saturation magnetization and magnetic susceptibility are several times larger than those of sample 6K#569R4-2 (Fig. 5b), but NRM intensity is less than 10 A/m (Fig. 5a). The estimated amount of titanomagnetite grains is 2.9 wt% based on the Curie temperature of 420 °C and Ms of 1.81 Am^2/kg. The seemingly inverse relationship of high amount of titanomagnetite and NRM, shown as high NRM for small amount (6K#569R4-2) and low NRM for large amount (6K#562R1), is mainly caused by distribution of the magnetic domain state, which is likely controlled by bulk lava flow cooling rate, not by total amount.

In contrast to fresh samples described above, 6K#569R4-1 is clearly hydrothermally altered, as indicated by sulfide mineralization, low CaO and K_2O contents, low density, and the dominance of paramagnetic minerals. The saturation magnetization of ferromagnetic minerals is extremely low, indicating that this sample contains much smaller amount of ferromagnetic minerals than the other samples (Fig. 5b). This is consistent with microscopic observations. Magnetic susceptibility of this sample is also very low (Fig. 5a). Only small amounts of ferromagnetic minerals exist in this sample, and they display a MD-like magnetic domain state. Pyrite and chalcopyrite grains are dominant and observed as grain

Fujii *et al. Earth, Planets and Space* (2018) 70:196

Page 12 of 14

assemblage with widths of 50–100 μm along cracks in the groundmass (Fig. 4C, D). These results indicate that fine titanomagnetite grains in groundmass are preferentially consumed and secondary sulfide minerals are crystallized during hydrothermal alteration processes. Iron in primary titanomagnetite could be moved to hydrothermal fluid, and iron and sulfur in secondary sulfides are derived from hydrothermal fluid. Although other possibilities such as silicate iron dissolution and seawater reduction as sulfur origin should be carefully considered, the absence of titanomagnetite grains in the samples studied here at least suggests that their alteration has supplied iron content into the fluid to promote secondary sulfide mineralization. Surely, the NRM intensity is less than 1 A/m on average (Fig. 5a), and the AFD result shows unstable remanence without linear trend (Fig. 6d). Moreover, NRM intensities are heterogeneous within cubic subsamples, indicating that the degree of alteration during hydrothermal processes differs spatially within lava flows. This is completely different from fresh samples of SD-like (6K#569R4-2) and MD-like (6K#562R1) end members, suggesting that igneous process cannot produce heterogeneity as seen in hydrothermal alteration process. The grain density of this sample (2.71 g/cm^3) is also lower than those of the two fresh samples (both 2.89 g/cm^3), which appears to be driven by the contribution of clay minerals. It is noteworthy that titanomagnetite grains in groundmass diminish along with considerable NRM reduction and sulfide mineralization in alteration halo, but hydrothermal alteration is not progressed in silicate phenocrysts (Fig. 4B). This result implies that main remanence carrier of fine titanomagnetite grains in groundmass were altered at an early stage of hydrothermal alteration. Sample 6K#569R4-3 can be classified as an example of partly altered volcanic rock in which hydrothermal fluid is reacted with titanomagnetite grains in groundmass. Fresh part shows the presence of titanomagnetite grains as shown in high values of saturation magnetization and microscope observation (Fig. 4I, J). In contrast, pyrite mineralization was observed in alteration halo and cracks in groundmass (Fig. 4G, H). Measured grain density value is as large as fresh samples (6K#562R1 and 6K#569R4-2), indicating that alteration of primary minerals and formation of clay minerals did not occur considerably. Thermomagnetic curves demonstrate that both comparatively fresh and oxidized areas coexist within this sample (Fig. 5d). The hysteresis measurements are consistent with these thermomagnetic results as only altered specimens show extremely low values of saturation magnetization and certain contribution of paramagnetic minerals ($N = 2$; Fig. 5b, d). Heterogeneity within the sample was also identified in

multi-specimen measurements of both NRM intensity and magnetic susceptibility (Fig. 4A). These results indicate that hydrothermal processes are party promoted and dissolve titanomagnetite grains in groundmass into solution. Self-reversed chemical remanent magnetization, which is produced during extreme low-temperature oxidation (maghemitization) of titanomagnetite by ionic reordering (Doubrovine and Tarduno 2006a), could be another cause of partly low values of NRM. However, it is indicated that very high oxidation states ($z > 0.9$) and relatively high Ti contents ($x > 0.6$) are needed to produce natural self-reversed components and that self-reversed magnetization (Doubrovine and Tarduno 2006b). Although oxidation states were not verified in this study, presented low x values of observed titanomagnetite grains (0.26 for 6K#562R1 and 6K#569R4-1 samples and 0.06 for 6K#569R4-3 sample; Table 3) at least suggested that self-reversal might not occur in studied samples.

Conclusions

Our analyses of basaltic andesites from the Irabu knolls clearly demonstrate that titanomagnetite grains in groundmass within back-arc lava flows are consumed in hydrothermal processes. Sulfides, such as pyrite and chalcopyrite, are crystallized as secondary minerals related to interaction with hydrothermal fluid. Fine grains of titanomagnetite can carry strong remanent magnetization, but may be easily consumed due to their small grain size. Therefore, the record of the geomagnetic field may be removed by hydrothermal alteration. Our results present NRM and susceptibility data for fresh and altered volcanic rock samples, providing an important benchmark for understanding marine magnetic anomaly related to seafloor hydrothermal circulation. Based on our results, magnetization reduction related to hydrothermal activity should produce local crustal magnetization lows and thus enables us to detect hydrothermal alteration zones by utilizing magnetic field measurements in space. In particular, the lavas we examined (via their resulting basaltic andesites) have high Curie temperature greater than 400 °C, which is significantly higher than those of mid-ocean ridge lavas, suggesting that the thermal effect for crustal magnetization may be less in back-arc settings. Therefore, the contrast between weakly magnetized hydrothermal alteration zones and magnetized surrounding lava flows may be clearly detected by magnetic anomalies even if magma and/or hydrothermal fluid (with near critical temperature) existed closer to target sites. The timing of magnetization reduction (titanomagnetite consumption and pyrite creation) due to hydrothermal alteration remains unresolved. Further investigation is needed to continue developing our understanding of

Fujii *et al. Earth, Planets and Space*   (2018) 70:196

Page 13 of 14

the duration and behavior of hydrothermal circulation in submarine volcanic systems.

Additional files

Additional file 1: Table S1. Data of bulk grain density, magnetic susceptibility, and natural remanent magnetization of each cube specimens extracted from studied lava flows.

Additional file 2: Table S2. Data of magnetic hysteresis parameters of each chip specimens extracted from studied lava flows.

Additional file 3: Table S3. Data of thermomagnetic curves of saturation magnetization in 50-700 °C.

Additional file 4: Figure S1. Backfield DC demagnetization curves of the studied lava samples; 6K#569R4-2, 6K#569R4-3, 6K#562R1, and 6K#569R4-1. The measurements were taken in limited field range to extract only remanent coercivity (Hcr). The 6K#569R4-3 sample display both fresh (solid line, top) and altered (broken line, bottom) specimens.

Abbreviations
AORI: Atmosphere and Ocean Research Institute; CMCR: Center for Advanced Marine Core Research; Hc: coercivity; Hcr: coercivity of remanence; MD: multidomain; PSD: pseudo-single domain; SD: single domain; LOI: loss on ignition; NRM: natural remanent magnetization; Ms: saturation magnetization; Mrs: saturation remanent magnetization; TRM: thermal remanent magnetization; VSM: vibrating sample magnetometer.

Authors' contributions
M.F. was involved in project planning, rock magnetics, and manuscript preparation. H.S. was involved in petrology, geochemistry, and manuscript preparation. E.T, K.S., and J.I. were involved in mineralogical measurements. All authors read and approved the final manuscript.

Author details
[1] National Institute of Polar Research, 10-3 Midoricho, Tachikawa, Tokyo 190-8518, Japan. [2] SOKENDAI (The Graduate University for Advanced Studies), Shonan Village, Hayama, Kanagawa 240-0193, Japan. [3] Senshu University, 2-1-1 Higashimita, Tama-ku, Kawasaki, Kanagawa 214-8580, Japan. [4] Kyushu University, 744 Motooka, Nishi-ku, Fukuoka 819-0395, Japan.

Competing interests
The authors declare that they have no competing interests.

Availability of data and materials
All magnetic and geochemical data are summarized in Tables 1, 2, 3, Additional file 2: Table S1, Additional file 3: Table S2 and Additional files 4: Table S3, and their details were described in the manuscript. Petrological and mineralogical features are given in Fig. 3.

Consent for publication
Not applicable.

Publisher's Note
Springer Nature remains neutral with regard to jurisdictional claims in published maps and institutional affiliations.

References
Ade-Hall JM, Palmer HC, Hubbard TP (1971) The magnetic and opaque petrological response of basalts to regional hydrothermal alteration. Geophys J R Astron Soc 24:137–174. https://doi.org/10.1111/j.1365-246X.1971.tb02171.x

Ade-Hall JM, Aumento F, Ryall PJC et al (1973) The mid-atlantic ridge near 45 °N. XXI. magnetic results from basalt drill cores from the median valley. Can J Earth Sci 10:679–696. https://doi.org/10.1139/e73-068

Alt JC (1995) Subseafloor processes in mid-ocean ridge hydrothennal systems. Seafloor hydrothermal systems: physical, chemical, biological, and geological interactions. AGU, Washington, pp 85–114

Caratori-Tontini F, Davy B, De Ronde CEJ, Embley RW, Leybourne M, Tivey MA (2012) Crustal magnetization of Brothers volcano, New Zealand, measured by autonomous underwater vehicles: geophysical expression of a submarine hydrothermal system. Econ Geol 107:1571–1581. https://doi.org/10.2113/econgeo.107.8.1571

Day R, Fuller M, Schmidt VA (1977) Hysteresis properties of titanomagnetites: grain-size and compositional dependence. Phys Earth Planet Inter 13:260–267. https://doi.org/10.1016/0031-9201(77)90108-X

Doubrovine PV, Tarduno JA (2006a) Alteration and self-reversal in oceanic basalts. J Geophys Res 111:B12S30. https://doi.org/10.1029/2006JB004468

Doubrovine PV, Tarduno JA (2006b) N-type magnetism at cryogenic temperatures in oceanic basalt. Phys Earth Planet Inter 157:46–54. https://doi.org/10.1016/j.pepi.2006.03.002

Dunlop DJ (2002) Theory and application of the Day plot (Mrs/Ms versus Hcr/Hc), 1. Theoretical curves and tests using titanomagnetite data. J Geophys Res Solid Earth 107:EPM4–1–EPM 4–22. https://doi.org/10.1029/2001JB000486

Fujii M, Okino K (2018) Near-seafloor magnetic mapping of off-axis lava flows near the Kairei and Yokoniwa hydrothermal vent fields in the Central Indian Ridge. Earth Planets Space 70:188. https://doi.org/10.1186/s40623-018-0959-5

Fujii M, Okino K, Honsho C, Dyment J, Szitkar F, Mochizuki N, Asada M (2015) High-resolution magnetic signature of active hydrothermal systems in the back-arc spreading region of the southern Mariana Trough. J Geophys Res Solid Earth 120:2821–2837. https://doi.org/10.1002/2014JB011714

Fukuba T, Noguchi T, Fujii T (2015) The Irabu Knoll: hydrothermal site at the eastern edge of the Yaeyama Graben BT. In: Ishibashi J, Okino K, Sunamura M (eds) Subseafloor biosphere linked to hydrothermal systems: TAIGA concept. Springer Japan, Tokyo, pp 493–496

Gee J, Kent DV (1997) Magnetization of axial lavas from the southern East Pacific Rise (14°-23°S): geochemical controls on magnetic properties. J Geophys Res 102:24873–24886. https://doi.org/10.1029/97JB02544

Halbach P, Nakamura K, Wahsner M, Lange J, Sakai H, Kaselitz L, Hansen R-D, Yamano M, Post J, Prause B, Seifert R, Michaelis W, Teichmann F, Kinoshita M, Marten A, Ishibashi J, Czerwinski S, Blum N (1989) Probable modern analogue of Kuroko-type massive sulphide deposits in the Okinawa Trough back-arc basin. Nature 338:496–499

Hall JM (1992) Interaction of submarine volcanic and high-temperature hydrothermal activity proposed for the formation of the Agrokipia, volcanic massive sulfide deposits of Cyprus. Can J Earth Sci 29:1928–1936. https://doi.org/10.1139/e92-150

Hannington MD, Jonasson IR, Herzig PM, Petersen S (1995) Physical and chemical processes of seafloor mineralization at mid-ocean ridges. Seafloor hydrothermal systems: physical, chemical, biological, and geological interactions. AGU, Washington, DC, pp 115–157

Haraguchi S, Ishizuka H, Ishii T, Fujioka K, Yuasa M, Shibasaki H (2014) Low- and high-T alteration of volcanics. Island Arc 23:324–343. https://doi.org/10.1111/iar.12078

Honsho C, Ura T, Kim K (2013) Deep-sea magnetic vector anomalies over the Hakurei hydrothermal field and the Bayonnaise knoll caldera, Izu-Ogasawara arc, Japan. J Geophys Res Solid Earth 118:5147–5164. https://doi.org/10.1002/jgrb.50382

Hunt CP, Moskowitz BM, Banerjee SK (1995) Magnetic properties of rocks and minerals. In: Ahrens TJ (ed) Rock Physics & Phase Relations: a handbook of physical constants. AGU Reference Shelf 3

Irving E (1970) The mid-atlantic ridge at 45° N. XIV. oxidation and magnetic properties of basalt; review and discussion. Can J Earth Sci 7:1528–1538. https://doi.org/10.1139/e70-144

Ishibashi J, Ikegami F, Tsuji T, Urabe T (2015) Hydrothermal activity in the Okinawa Trough back-arc basin: geological background and hydrothermal mineralization. In: Ishibashi J, Okino K, Sunamura M (eds) Subseafloor biosphere linked to hydrothermal systems: TAIGA concept. Springer, Japan, Tokyo, pp 337–359. https://doi.org/10.1007/978-4-431-54865-2_27

Johnson HP, Merrill RT (1972) Magnetic and mineralogical changes associated with low-temperature oxidation of magnetite. J Geophys Res 77:334–341. https://doi.org/10.1029/JB077i002p00334

Johnson HP, Merrill RT (1973) Low-temperature oxidation of a titanomagnetite and the Implications for paleomagnetism. J Geophys Res 78:4938–4949. https://doi.org/10.1029/JB078i023p04938

Johnson HP, Karsten JL, Vine FJ, Smith GC, Schonharting G (1982) Low-level magnetic survey over a massive sulfide ore body in the Troodos ophiolite complex, Cyprus. Mar Technol Soc J 16:76–80

Letouzey J, Kimura M (1986) The Okinawa Trough: genesis of a back-arc basin developing along a continental margin. Tectonophysics 125:209–230. https://doi.org/10.1016/0040-1951(86)90015-6

Mottle MJ, Holland HD (1978) Chemical exchange during hydrothermal alteration of basalt by seawater—I. Experimental results for major and minor components of seawater. Geochim Cosmochim Acta 42(8):1103–1115. https://doi.org/10.1016/0016-7037(78)90107-2

Sato H (2010) Quantitative analyses with X-ray fluorescence analyzer of major elements for rock samples. Bull Ins Natur Sci Senshu Univ 41:15–23 **(in Japanese)**

Sibuet JC, Letouzey J, Barbier F, Charvet J, Foucher JP, Hilde TWC, Kimura M, Chiao LY, Marsset B, Muller C, Stéphan JF (1987) Back arc extension in the Okinawa Trough. J Geophys Res Solid Earth 92:14041–14063. https://doi.org/10.1029/JB092iB13p14041

Tivey MA, Rona PA, Schouten H (1993) Reduced crustal magnetization beneath the active sulfide mound, TAG hydrothermal field, Mid-Atlantic Ridge at 26°N. Earth Planet Sci Lett 115:101–115. https://doi.org/10.1016/0012-821X(93)90216-V

Watkins ND, Paster TP (1971) The magnetic properties of igneous rocks from the ocean floor. Philos Trans R Soc London A Math Phys Eng Sci 268:507–550

Zhou W, van der Voo R, Peacor DR, Wang D, Zhang Y (2001) Low-temperature oxidation in MORB of titanomagnetite to titanomaghemite: a gradual process with implications for marine magnetic anomaly amplitudes. J Geophys Res 106:6409–6421. https://doi.org/10.1029/2000JB900447